

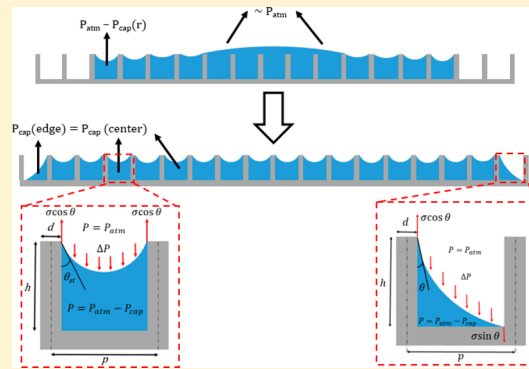
Dynamics of Microscale Liquid Propagation in Micropillar Arrays

Mohamed H. Alhosani^{ID} and TieJun Zhang*

Department of Mechanical and Materials Engineering, Masdar Institute, Khalifa University of Science and Technology, Post Office Box 54224, Abu Dhabi, United Arab Emirates

Supporting Information

ABSTRACT: Understanding the dynamics of microscale liquid propagation in micropillar arrays can lead to significant enhancement in macroscopic propagation modeling. Such a phenomenon is fairly complicated, and a fundamental understanding is lacking. The aim here is to estimate three main parameters in liquid propagation, capillary pressure, average liquid height, and contact angle on the pillar side, through modeling and experimental validation. We show that the capillary pressure is not constant during liquid propagation, and the average capillary pressure is evaluated using its maximum and minimum values. The average liquid height influences the permeability of such a structure, which is challenging to determine as a result of the complicated three-dimensional (3D) meniscus shape. A simple physical model is provided in this paper to predict the average liquid height with less than 7% error. The contact angle on the micropillar side, which has considerable impact on the capillary pressure and the average liquid height, has been debated for a long time. We propose a model to predict this contact angle and validate it against experimental values in the literature. Our findings also indicate that the microscopic motion of the liquid front is significantly affected by the ratio of the pillar height to edge-to-edge spacing, and a correlation is provided for quantification. The proposed models are able to predict the droplet spreading dynamics and estimate spreading distance and time reasonably.



Downloaded via UNIV OF OSLO on September 4, 2018 at 17:17:28 (UTC).
See https://pubs.acs.org/sharingguidelines for options on how to legitimately share published articles.

1. INTRODUCTION

Liquid propagation (wicking) in porous media has been extensively studied, owing to its application in a variety of engineering applications, such as thermal management of high heat flux devices, microfluidics, and power generation. The advantage of such surfaces is that capillary pressure provides an effective liquid transport mechanism for small devices. These surfaces can be produced by introducing micro-/nanostructures on intrinsically hydrophilic surfaces based on the Wenzel equation.¹ Among these surfaces, silicon micropillar arrays have been extensively studied to understand the fundamentals of liquid propagation.^{2–7} Using a photolithography technique and deep reactive ion etching (DRIE), a precise pillar diameter, spacing, and height can be manufactured, which is crucial for a fundamental understanding. Also, a scalable and low-cost micro-/nanostructured surface can be fabricated on metallic surfaces using different methods, such as anodization,^{8,9} oxidation,³ electrochemical deposition,^{3,8} and biotemplated nanofabrication.¹⁰

One of the early studies in liquid propagation was performed by Washburn¹¹ to estimate the liquid rise rate in capillary tubes. The model was obtained by balancing the capillary pressure with viscous resistance, which was then extended to predict liquid propagation in porous media. The main challenge in such a problem is to estimate the capillary pressure and viscous resistance (permeability). Recently, Xiao et al.¹² proposed a semi-analytical model to predict the liquid propagation rate in a

micropillar array. The capillary pressure was determined by predicting the meniscus shape using energy minimization software called “surface evolver” and validated using interferometry (confocal microscope images). Brinkman’s equation was solved numerically to obtain permeability. The model provides good predictions when the height to spacing ratio is larger than 1 and the diameter to spacing ratio is lower than 0.57 and overpredicts outside this range. To overcome this problem, the same group¹³ studied the microscale liquid propagation dynamics, in which the liquid propagation between two pillars (sweeping) was analyzed. The results show the importance of accounting for microscale dynamics, especially in sparse structures. They also show that the sweeping distance scales with one-fifth power of time. Another study performed by Tanner suggests that the sweeping distance scales with one-seventh power of time.¹⁴

Rahman et al.¹⁰ studied the effect of the liquid propagation rate on critical/dryout heat flux. The propagation rate was measured with high-speed imaging of liquid drawn from a 500 μm capillary tube when in contact with the surface. The results show that the liquid propagation rate is the single main factor that determines the dryout heat flux on structured superhydrophilic surfaces. Optimization of liquid propagation on square micropillar arrays

Received: March 30, 2017

Revised: May 25, 2017

Published: May 31, 2017



ACS Publications

© 2017 American Chemical Society

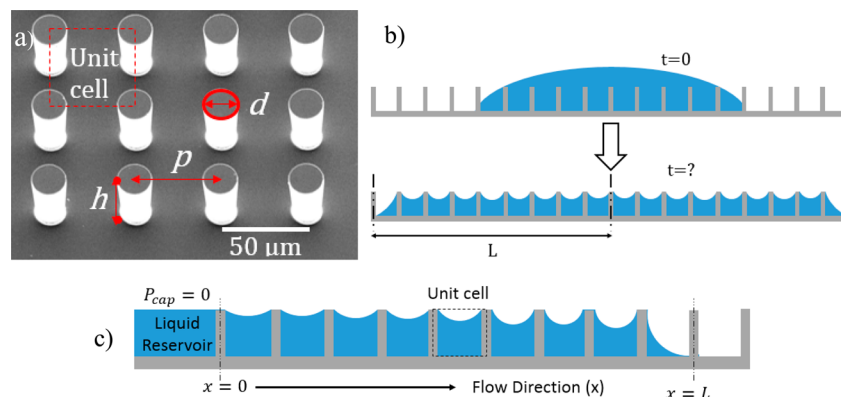


Figure 1. (a) SEM image of the fabricated sample with diameter d , pitch p , and height h , (b) schematics of droplet spreading in micropillar arrays, and (c) side-view schematic of liquid propagation in micropillar arrays.

was performed by Hale et al.¹⁵ based on several models and numerical simulations. It was found that, for a given aspect ratio, there exists an optimum pillar spacing that provides the maximum flow rate. Another group also presented the dynamics of liquid propagation in nanopillars¹⁶ and reported that pillar structures have significant influence on the propagation process. The modeling results were then validated with experimental data from the literature. Antao et al.¹⁷ provided a simple yet accurate capillary pressure model based on the force balance in a unit cell of a micropillar array. The model was used to estimate the maximum propagation rate, which is also a representation of the dryout heat flux on such surfaces.¹⁸

Despite the huge effort directed to understand the liquid propagation in micro-/nanostructured surfaces, this phenomenon is still unclear, and different models produce various results, as shown by Horner et al.⁴ and Ravi et al.^{19,20} For instance, the microscopic sweeping process is still vague, and physical insight of this process can lead to significant improvement in the macroscopic behavior. Also, an important parameter to simulate liquid propagation is the contact angle on the pillar side, which was determined by interferometry by Antao et al.,¹⁷ for water on silicon to be much larger than the equilibrium contact angle. Also, Ravi et al.^{19,20} used a contact angle of 56° when simulating water propagation on a silicon micropillar array. On the other hand, Zhu et al.¹⁸ used a contact angle of 30°. This shows that a model that can predict the contact angle of liquid on the micropillar side is lacking in the literature.

Another important parameter that affects the liquid propagation rate is the permeability. One of the early studies to estimate permeability of a micropillar arrays was performed by Sangani and Acrivos in 1982.² The proposed numerical model assumes a flat meniscus (contact angle of 90°) between the pillars, which lead to overprediction of permeability because the liquid flow area is larger. The effect of meniscus curvature was taken into account on the Byon and Kim³ permeability model, in which the surface energy minimization tool was used to obtain a general correlation for the average meniscus height. One main drawback is that this correlation can be significantly off if the parameters used are not within the range of the correlation. Recently, Zhu et al.¹⁸ proposed that the meniscus height/curvature is changing from the liquid supply point along the wicking direction. Basically, the pressure difference in the wicking system is due to the curvature difference. This change in curvature results in different meniscus heights along the flow. Therefore, a simple universal model is needed to accurately predict the average (effective) meniscus height within a unit cell

as a function of the pillar diameter, spacing, height, and contact angle.

In this paper, we show that the capillary pressure during propagation and sweeping is not constant, and therefore, the average capillary pressure is proposed on the basis of the maximum and minimum capillary pressures. Also, a model that can predict the contact angle on the micropillar sidewall was produced and validated against interferometry measurements from the literature. Furthermore, we provide a simple yet accurate model to estimate the average liquid height in a unit cell, which is crucial for permeability estimation. Finally, the average capillary pressure, average liquid height, and contact angle models were validated using liquid rise and droplet spreading experiments on silicon micropillar arrays.

2. RESULTS AND DISCUSSION

In this work, we study the liquid propagation in hydrophilic micropillar arrays. A scanning electron microscopy (SEM) image of such a sample with a pillar diameter of d , center-to-center spacing (pitch) of p , and pillar height of h is shown in Figure 1a. The aim is to estimate the spreading time and spreading diameter when a liquid droplet is deposited on such surfaces (Figure 1b) and also to predict the liquid propagation rate when such a surface comes in contact with the liquid reservoir, as shown in Figure 1c.

Darcy's law for flow in porous media can be used to simulate this problem

$$\dot{m}_{\text{prop}} = -\frac{\rho K A}{\mu} \frac{dP}{dx} \quad (1)$$

where \dot{m}_{prop} is the liquid mass flow rate, ρ is the liquid density, K is the permeability, A is the liquid flow area, and μ is the liquid viscosity. The driving pressure in this case is the capillary pressure (P_{cap})

$$\frac{dP}{dx} = \frac{(P_{\text{atm}} - P_{\text{cap}})_{x=L} - (P_{\text{atm}} - P_{\text{cap}})_{x=0}}{L} \quad (2)$$

where L is the propagating distance from the liquid reservoir. To estimate the liquid propagation rate, we need to obtain the permeability and capillary pressure.

2.1. Average Capillary Pressure in Micropillar Arrays.

When liquid is moving from one row of pillars to the next row, the capillary pressure is not constant. For instance, the maximum capillary pressure is just after the liquid wets the micropillars, and the minimum capillary pressure (P_{min}) is just before the liquid

wets the next row of pillars. Applying the force balance in a unit cell of micropillar arrays suggests that capillary pressure follows the equation below (see section S-1 of the Supporting Information for the derivation)

$$P_{\text{cap}}(x) = \frac{\sigma \frac{\pi d}{2} \cos \theta_{\text{adv}} - p \sigma \sin \theta_{\text{adv}}}{p \left(\frac{d}{2} + x \right) - \frac{\pi d^2}{8}} \quad (3)$$

where θ_{adv} is the advancing contact angle and x is the distance from the pillar edge to the liquid front. Note that the pressure difference (ΔP) in Figure 2 is equal to P_{cap} . As a result of the

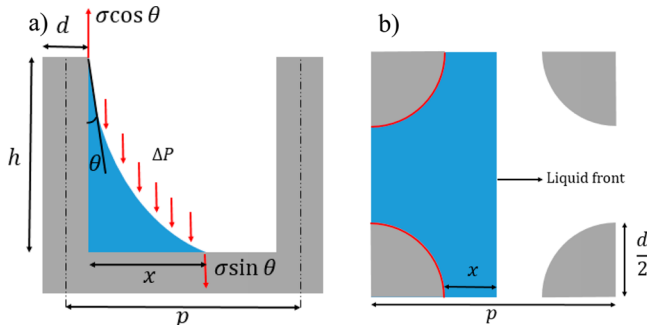


Figure 2. (a) Side view and (b) top view of the liquid front and forces on the meniscus during the sweeping process.

DRIE process, scallop-like structures are formed on the pillar side, which should result in a lower contact angle based on the Wenzel equation. However, high-resolution SEM images show that pillar-side roughness is equal to 1.01–1.02, which can be neglected (see section S-1 of the Supporting Information for an image). Other studies also show similar results, such as that from Ayon et al.²¹ However, this roughness can be changed by changing DRIE process parameters.

We define P_{max} when the liquid front at $x = 0$ and P_{min} when $x = p - d$, as shown in Figure 3.

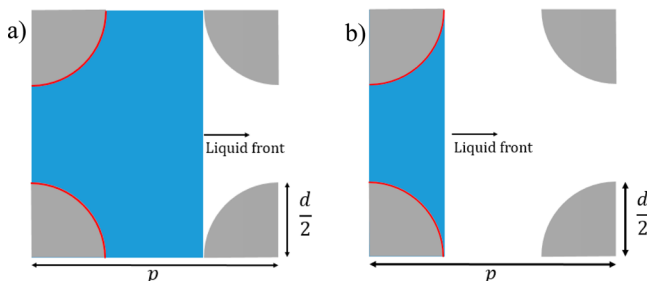


Figure 3. Top view of the liquid front location when the capillary pressure is equal to (a) P_{min} and (b) P_{max} .

With substitution of the value of x in eq 3, P_{min} and P_{max} can be calculated as shown in eqs 4 and 5, respectively.

$$P_{\text{min}} = \frac{\sigma \frac{\pi d}{2} \cos \theta_{\text{adv}} - p \sigma \sin \theta_{\text{adv}}}{p \left(p - \frac{d}{2} \right) - \frac{\pi d^2}{8}} \quad (4)$$

$$P_{\text{max}} = \frac{\sigma \frac{\pi d}{2} \cos \theta_{\text{adv}} - p \sigma \sin \theta_{\text{adv}}}{p \left(\frac{d}{2} \right) - \frac{\pi d^2}{8}} \quad (5)$$

The above model does not take into account the effect of the pillar height on the capillary pressure because it did not appear in the force balance directly. Previous studies reported overestimation of the capillary pressure when short pillars are modeled.¹³ The main parameter here is the ratio of the pillar height to edge-to-edge spacing [$h/(p - d)$]. When $h/(p - d) < 1$, the capillary pressure is overestimated. The reason is that the contact angle on the pillar side (θ_{pillar}) is not the same as θ_{adv} for short pillars. Basically, for very short pillars, it is physically impossible to have θ_{adv} on both the bottom surface and pillar side, as shown in Figure 4.

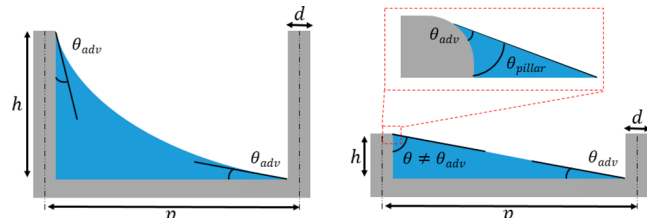


Figure 4. Liquid meniscus and contact angle on long and short pillars.

To estimate θ_{pillar} from $h/(p - d)$, two boundary conditions are used. If $h = (p - d)$, both the bottom surface and pillar side contact angle will equal θ_{adv} . On the other hand, if the pillar height approaches zero, θ_{pillar} will approach $(90 + \theta_{\text{adv}})$. Note that the contact angle on the pillar wall can be larger than θ_{adv} as a result of the edge effect on the pillar top, which does not exist on the bottom surface, as shown in Figure 4. On the basis of these two boundaries, an approximation is developed to estimate θ_{pillar} from $h/(p - d)$, as shown below.

$$\theta_{\text{pillar}} = 90 - 2 \tan^{-1} \left(\frac{h}{p - d} \right) + \theta_{\text{adv}} \quad (6)$$

Because θ_{pillar} cannot be lower than θ_{adv} , $\max[\theta_{\text{pillar}}, \theta_{\text{adv}}]$ is substituted in the first term of eqs 3 and 4.

During the liquid propagation process, the average capillary pressure can be determined from the time average of the pressure along x . A previous study by Xiao et al.¹³ shows that the liquid front location (x) is a function of $t^{1/5}$, where t is the time. However, Tanner¹⁴ reported that x is a function of $t^{1/7}$. The first study that states the sweeping distance scaling as $t^{1/5}$ was performed on silicon micropillar arrays. The second study, on the other hand, was on a smooth surface. In the case of silicon micropillar arrays, the meniscus is pinned at the pillar top with a constant height, while in the second case, the liquid thickness decreases. This implies that the pillar height affects the sweeping distance scaling (β), where $x = f(t^\beta)$. Therefore, six samples are tested, and the liquid (water) sweeping on plasma-cleaned silicon micropillar array samples with $h/(p - d)$ ranges between 0.5 and 1.6 is recorded with a high-speed camera at 5000 frames per second. It was found that $h/(p - d)$ strongly affects β , and a correlation is developed to estimate β from $h/(p - d)$, as shown below (Figure 5). While this correlation is valid for the experimented range of $h/(p - d)$, we do not expect β to keep increasing. There is a physical limitation in which β cannot go beyond that, which will be discussed later in this paper.

$$\beta = 0.2705 \left(\frac{h}{p - d} \right) + 0.0784 \quad (7)$$

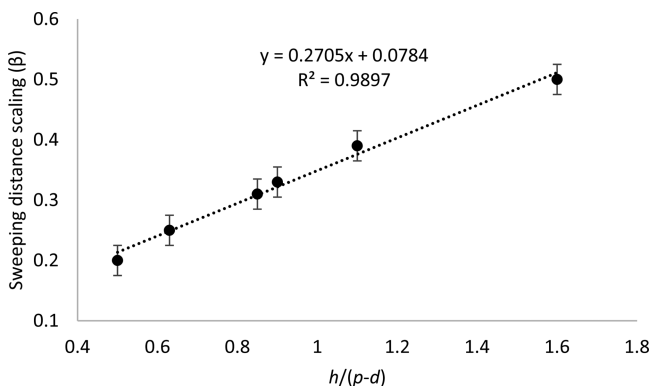


Figure 5. Sweeping distance scaling (β) versus $h/(p-d)$.

Using this information, the average capillary pressure (P_{avg}) can be determined, as shown below (see section S-3 of the Supporting Information for the derivation)

$$P_{\text{avg}} = \sum_{i=1}^{i=t_s/dt} \frac{A}{Bt(i)^{\beta} + C} dt \quad (8)$$

where

$$\begin{aligned} A &= \sigma \frac{\pi d}{2} \cos \theta_{\text{pillar}} - p \sigma \sin \theta_{\text{adv}}, \quad B = p(p-d), \\ C &= \frac{pd}{2} - \frac{\pi d^2}{8} \end{aligned}$$

The above model was for the edge unit cells. If we consider a unit cell with all four pillars wetted (center unit cell), the capillary pressure can be determined as that in ref 17 (see section S-2 of the Supporting Information for more details).

$$P_{\text{center}} = \frac{4\sigma \cos \theta}{d \left(\frac{4}{\pi} \left(\frac{p}{d} \right)^2 - 1 \right)} \quad (9)$$

We can use the above results to explain different phenomena, such as the liquid receding mechanism, in micropillar arrays. Considering the silicon micropillar array with $d = 25$, $p = 65$, $h = 36 \mu\text{m}$ and the contact angle of plasma-cleaned silicon/silicon dioxide of about 2° , the capillary pressure versus liquid front location (x) is illustrated in Figure 6.

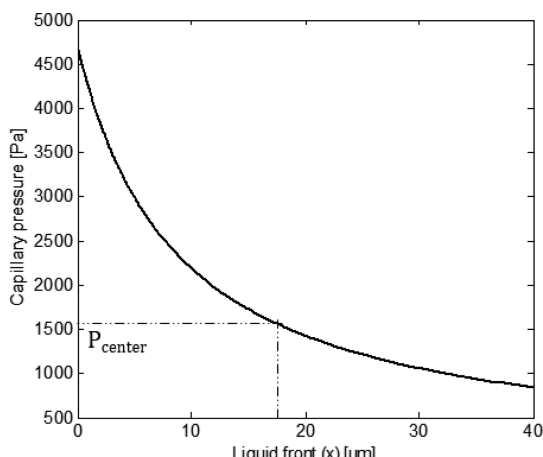


Figure 6. Capillary pressure variation in the edge unit cell for $d = 25$, $p = 65$, $h = 36 \mu\text{m}$, and $\theta_{\text{eq}} = 2^\circ$.

From Figure 6, during evaporation and the liquid front receding process, the liquid front (x) cannot be below the point that generates capillary pressure equal to $P_{\text{center,max}}$ [P_{center} when $\theta = \text{receding contact angle } (\theta_{\text{rec}})$], which, in this case, is equal to $17 \mu\text{m}$. The reason is that, when looking at the unit cell just before the edge unit cell (let us call it “unit cell A” in Figure 7a), which has four pillars wetted with water, the maximum capillary pressure that can be generated is $P_{\text{center,max}}$. Assuming a negligible pressure drop between the unit cell A and edge unit cell, the liquid front in the edge unit cell will recede until it reaches the point where the capillary pressure in the edge unit cell is equal to the maximum capillary pressure of unit cell A, which is $P_{\text{center,max}}$. At this point, the liquid front in the edge unit cell will stop receding and the meniscus will depin and recede from the pillar top in the unit cell A until the bottom of the meniscus touches the substrate bottom surface, as shown in Figures 7a and 8. The analysis also indicates that the drying process similar to Figure 7b is not possible. The reason is that, to completely remove liquid from the edge unit cell, the pressure in the unit cell A should be larger than P_{max} , which is not possible.

Experimental observations also support this, as shown in Figure 9. The optical microscopic images were taken after depositing the water droplet on the surface and waiting for about 1 min until the drying process is observed. The liquid front distance, x , was measured to be about $16 \mu\text{m}$ in this experiment, which validates the capillary pressure model. Also, the proposed drying process in Figure 7a agrees with the experimental drying process in Figure 9.

The same argument can be used to estimate the maximum sweeping distance scaling (β_{max}), which is to make $P_{\text{avg}} = P_{\text{center,max}}$ and solve for β . Therefore, for the tested sample above, $\beta_{\text{max}} \sim 0.75$.

One particular importance of $P_{\text{center,max}}$ is that it determines the capillary pressure at dryout heat flux for cooling applications.¹⁸ Basically, the liquid is pumped by capillary pressure from the liquid pool to the heated section, and cooling is happening by evaporation of liquid in the heated section. The maximum cooling capacity of such a device is a direct function of the maximum liquid supply rate, that is, when $P_{\text{cap}} = P_{\text{center,max}}$. The analysis in this paper suggests that the capillary pressure in propagating liquid (P_{avg}) is different from the capillary pressure of a receding liquid (P_{center}). Because P_{center} is relatively easier to estimate because the liquid front motion (x versus t) is not required, a correlation was developed to estimate P_{avg} from $P_{\text{center,max}}$, $h/(p-d)$, and porosity (ε) (see section S-3 of the Supporting Information for details).

$$P_{\text{avg}} = P_{\text{center,max}} \left[0.469 + \frac{0.774h}{p-d} - 0.3582\varepsilon - 0.3 \left(\frac{h}{p-d} \right)^2 + 0.128 \frac{\varepsilon h}{p-d} + 0.0176\varepsilon^2 \right] \quad (10)$$

$$\varepsilon = \frac{p^2 - \frac{\pi d^2}{4}}{p^2} \quad (11)$$

The correlation in eq 10 is valid for $0.35 < \varepsilon < 0.9$ and $0.5 < h/(p-d) < 1.6$ for structures similar to micropillar arrays and produces results with less than 5% error when compared to the solution in eq 10. Note that the disjoining pressure is neglected in this work as a result of the relatively large length scale of the

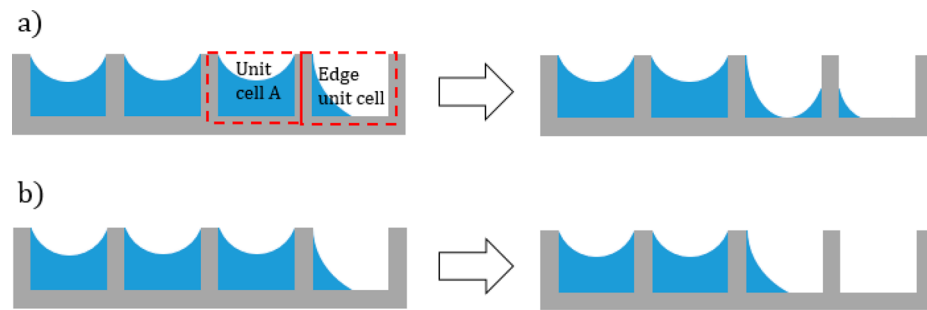


Figure 7. Dynamics of drying of the micropillar array surface: (a) possible and (b) not possible.

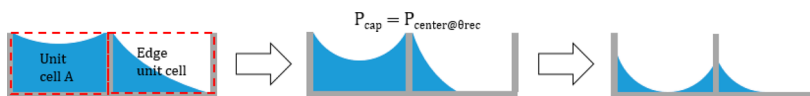


Figure 8. Dynamics of liquid drying/receding.

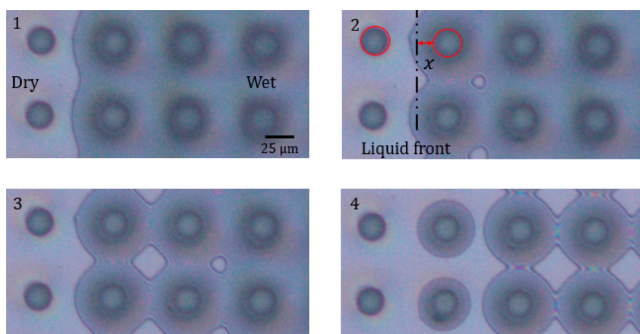


Figure 9. Optical microscopic images of dynamic liquid front receding in the micropillar array surface, with $d = 25$, $p = 65$, $h = 36 \mu\text{m}$, and $\theta_{\text{adv}} = 2^\circ$.

structures. To apply this model to nanopillars and nanowires with sub-micrometer length scale, an order of magnitude analysis should be performed to determine how significant the disjoining pressure is compared to the capillary pressure. A comparison between the capillary pressure model prediction of this work and those of Xiao et al.¹² and Srivastava et al.²² is presented in section S-3 of the Supporting Information.

2.2. Contact Angle on the Pillar Side. Now, we will consider depositing a droplet on micropillar arrays. Liquid is propagated from the central region (droplet region), where the pressure is equal to atmospheric pressure P_{atm} (capillary pressure of ~ 0), to the thin-film region, where the pressure is equal to $P_{\text{atm}} - P_{\text{avg}}$. A steady state (no flow) happens when the pressure difference is zero. Therefore, the pressure on the edge unit cells calculated by eq 4 should equal the pressure in the middle region,

which is calculated using eq 9, with the contact angle equal to the steady-state contact angle (θ_{st}), as shown in Figure 10.

We have seen before that the edge capillary pressure is not constant and is fluctuating between P_{\min} and P_{\max} . Also, the capillary pressure in the central region is increasing from about 0 (when the droplet is deposited and we have a flat meniscus) to the point that the center pressure is equal to the edge pressure. A steady state (no flow) happens when the pressure difference between the edge and center is zero. The first point that will satisfy the no-flow condition is when $P_{\text{edge}} = P_{\min}$, which indicates that the liquid front in the edge unit cell is as indicated in Figure 3a, which is the minimum capillary pressure of the edge unit cell. Optical microscopic visualization of the liquid front directly after droplet deposition shows that the liquid front is very close to the next row of pillars (which produce P_{\min}), as shown in Figure 11, which reflects the modeled scenario.

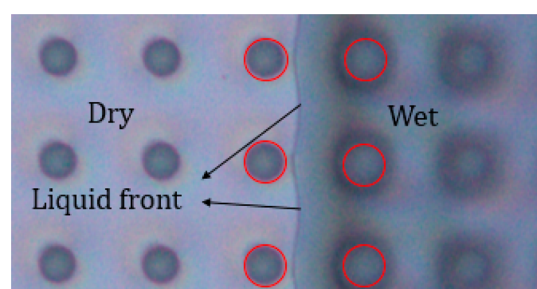


Figure 11. Optical microscopic visualization of the liquid front at a steady state.

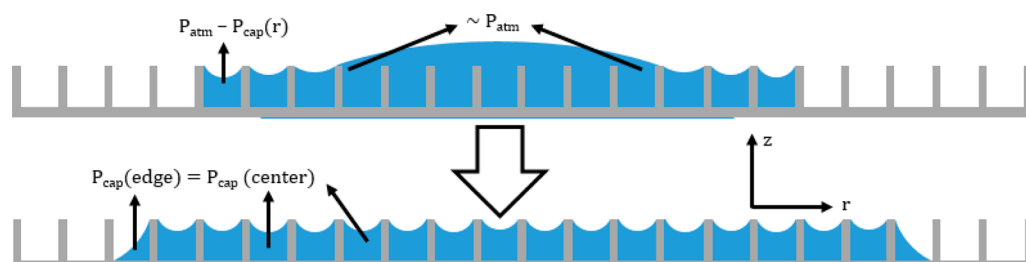


Figure 10. Droplet spreading on a superhydrophilic micropillar arrays. A steady state happens when the central pressure is equal to the edge pressure.

When P_{\min} ($\theta = \theta_{\text{adv}}$) in eq 4 equals P_{center} ($\theta = \theta_{\text{st}}$) in eq 9, θ_{st} in the middle region can be calculated as follows (see section S-2 of the Supporting Information for the derivation):

$$\theta_{\text{st}} = \cos^{-1} \left(\frac{P_{\min} d \left(\frac{4}{\pi} \left(\frac{p}{d} \right)^2 - 1 \right)}{4\sigma} \right) \quad (12)$$

This is the contact angle on the sides of all pillars (except edge pillars, in which $\theta = \theta_{\text{adv}}$) when the liquid stops propagating with a negligible evaporation rate. This explains why the water contact angles on silicon micropillar sides are larger than the equilibrium contact angle on a smooth silicon surface.^{4,17,19,20} For example, Antao et al.¹⁷ used a confocal measurement to estimate the contact angle on a silicon micropillar, and a value of $50^\circ \pm 4^\circ$ was reported. Using the same pillar geometry, our model predicts a contact angle of 58° .

2.3. Average Liquid Height. To estimate the spreading diameter of a drop when deposited in micropillar arrays, and to estimate the permeability of such structure, the liquid height should be estimated. This can be achieved by applying horizontal force balance in a unit cell as shown in Figure 12 below.

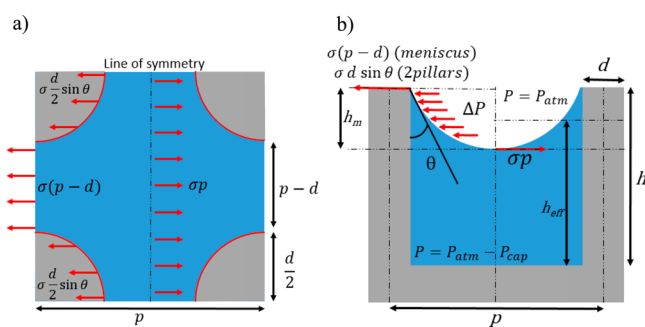


Figure 12. (a) Top view and (b) side view of horizontal forces acting on the half unit cell.

At steady state, forces toward the left should equal forces toward the right, and solving that will lead to (see section S-4 of the Supporting Information for the derivation)

$$h_m = \frac{\sigma(1 - \sin \theta)}{P_{\text{cap}}} \left(\frac{d}{p} \right) \quad (13)$$

where h_m is the meniscus height. The effective meniscus height from the bottom surface is

$$h_{\text{eff}} = \left(h - \frac{h_m}{2} \right) \quad (14)$$

To validate our model in eqs 13 and 14, four silicon micropillar array samples were fabricated and four experiments were performed for each sample. Therefore, each experimental result in Table 1 is the average of four experiments. Before the

experiment, the sample is cleaned with acetone, isopropyl alcohol (IPA), water, and 20 min of plasma cleaning. The contact angle after plasma cleaning was measured to be around 2° . The droplet is generated using a 32 gauge size needle that can produce a droplet size ranging from 1 to $3 \mu\text{L}$. To accurately measure the droplet size, a high-speed camera was used to take side-view images of the droplet, as shown in Figure 13a. The high-speed

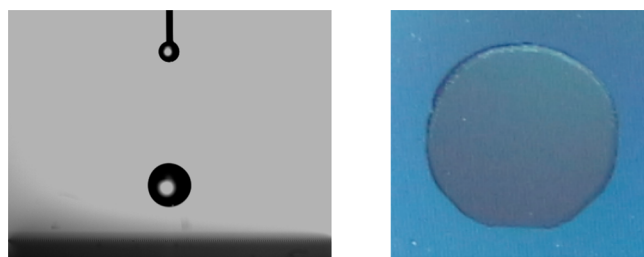


Figure 13. (a) Side-view image with a high-speed camera and (b) top-view image of the final wetted area.

camera video was also used to measure spreading time, which will be discussed in the next section. Another camera was used to take a top-view image, so that the final wetted area can be measured, as in Figure 13b. The time between the droplet contacting the surface and top-view image is about 2–3 s, and during this short period, evaporation is neglected. For instance, a $2 \mu\text{L}$ droplet needs more than 2 min to completely evaporate under lab conditions. ImageJ software was used to measure the droplet volume (side-view image) and wetted area (top-view image). To estimate the wetted area, the liquid volume in each unit cell (V_{Lcell}) should be calculated using h_{eff} as shown below.

$$V_{\text{Lcell}} = p^2 h_{\text{eff}} - \pi \left(\frac{d}{2} \right)^2 h_{\text{eff}} \quad (15)$$

Because this problem represents a steady-state condition (no flow), the contact angle on all pillars will equal to θ_{st} , and P_{cap} will equal to P_{\min} , which is substituted in eq 13. If the liquid volume in each unit cell is known, the final wetted area can be calculated from the initial droplet volume (V_i).

$$A_{\text{wetted}} = \frac{V_i}{V_{\text{Lcell}}} p^2 \quad (16)$$

Our model prediction is compared to the Byon and Kim model³ in Table 1, which shows significant improvement. Note that θ_{adv} is substituted in the Byon and Kim model, and if θ_{st} is used instead, both model produce almost the same results with less than 7% error.

2.4. Validation with the Capillary Liquid Rise Experiment. P_{avg} and h_{eff} models can be validated using liquid rise rate experiments. However, h_{eff} is changing from the liquid pool to the liquid front, as indicated by Zhu et al.¹⁸ For instance, at $z = 0$, we have a flat meniscus with zero capillary pressure, and therefore, $h_{\text{eff}} = h$. At the other end, where $z = L$, the capillary pressure is

Table 1. Experimental and Modeling Results of the Liquid Volume in a Unit Cell

d, p , and h (μm)	θ_{adv}	θ_{st}	experimental V_{Lcell} (pL)	modeled V_{Lcell} (pL)	percent error (%)	Byon and Kim V_{Lcell} (pL) ³	percent error (%)
14, 36, and 35.7	2	56.2	38.7 ± 1.0	39.0	0.9	34.2	11.6
19, 51, and 35.6	2	56.5	73.4 ± 2.5	77.5	5.6	63.6	13.4
24, 66, and 35.6	2	57.5	119.8 ± 2.1	128.3	7.1	97.7	18.4
34, 76, and 37.9	2	55.4	160.2 ± 4.6	169.0	5.5	126.2	21.2

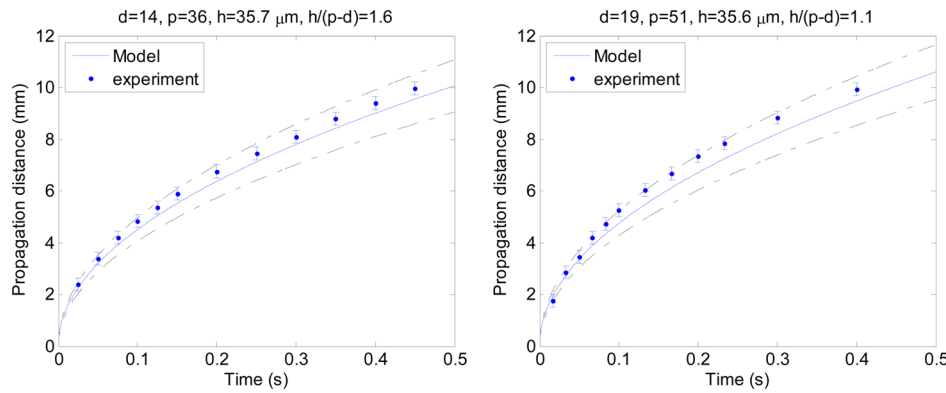


Figure 14. Propagation distance versus time in micropillar arrays: (a) $d = 14$, $p = 36$, and $h = 35.7 \mu\text{m}$ and (b) $d = 19$, $p = 51$, and $h = 35.6 \mu\text{m}$. Dashed lines are $\pm 10\%$ error.

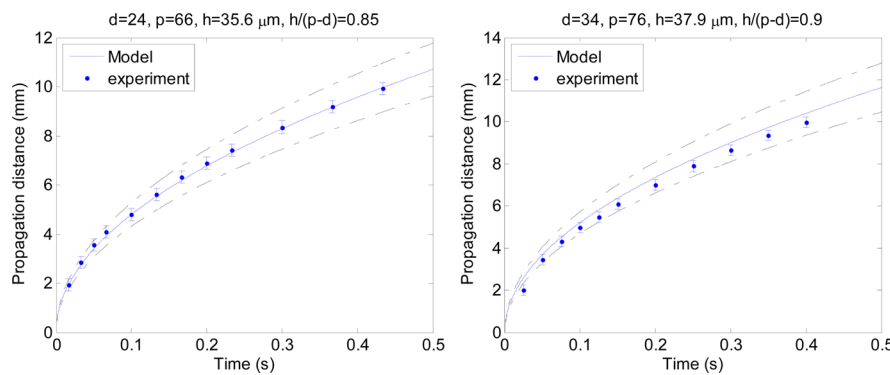


Figure 15. Propagation distance versus time in micropillar arrays: (a) $d = 24$, $p = 66$, and $h = 35.6 \mu\text{m}$ and (b) $d = 34$, $p = 76$, and $h = 37.9 \mu\text{m}$. Dashed lines are $\pm 10\%$ error.

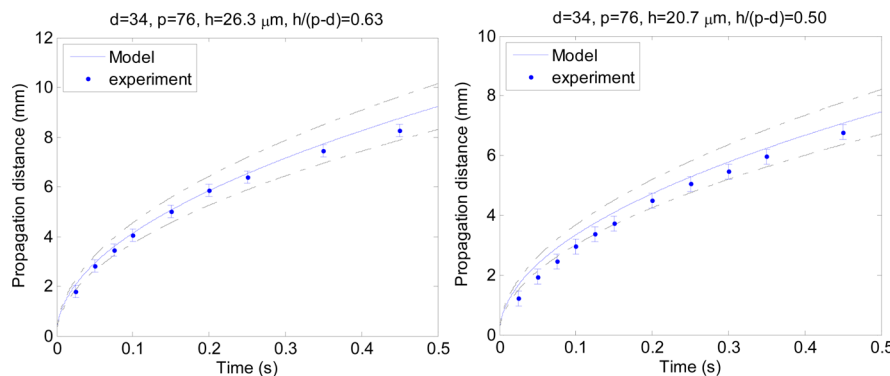


Figure 16. Propagation distance versus time in micropillar arrays: (a) $d = 35$, $p = 75$, and $h = 26.3 \mu\text{m}$ and (b) $d = 35$, $p = 75$, and $h = 20.7 \mu\text{m}$. Dashed lines are $\pm 10\%$ error.

equal to P_{avg} , which is used to estimate the contact angle using eq 12. After that, this contact angle and P_{avg} is used to calculate h_{eff} using eqs 13 and 14. An average value of h_{eff} is taken, as shown below.

$$h_{\text{avg}} = \frac{h + h_{\text{eff}}}{2} \quad (17)$$

h_{avg} was then substituted in the Byon and Kim model (see section S-4 for equation) to obtain the permeability.³ Equation 1 can be solved to obtain the propagation distance as a function of time, as shown below

$$z = \sqrt{\frac{2KP_{\text{avg}}t}{\mu\epsilon}} \quad (18)$$

where z is the propagation distance and t is the time. The experiment starts when the vertically oriented silicon micropillar arrays sample comes in contact with the water pool. Note that gravity is neglected in this study because the capillary pressure for this structure is more than 10 times larger than the static head at the maximum propagation distance. The propagation distance versus time was measured using a high-speed camera at 200 frames per second (Figures 14–16). Before the experiment, the samples were cleaned with acetone, IPA, water, and then 20 min of plasma cleaning. The experiments were performed in lab conditions with the temperature of $\sim 25^\circ\text{C}$. Our models agree with the experimental results with less than 10% error.

2.5. Droplet Spreading in Silicon Micropillar Arrays.

When a droplet is deposited on a nano-/microstructured surface,

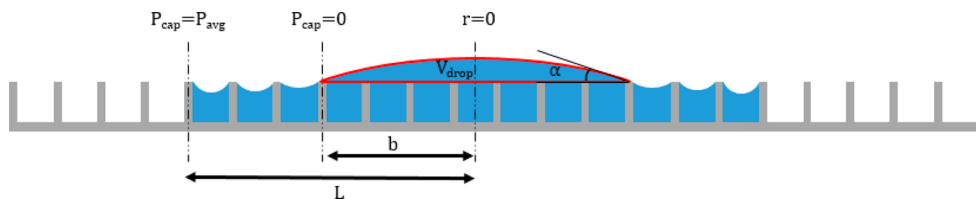


Figure 17. Schematic of droplet spreading on a micropillar array surface (thin-film region: r between b and L).

liquid propagates from the droplet region to the thin-film region as a result of the pressure difference. The liquid pressure in the droplet region is about the atmospheric pressure (P_{atm}), while in the thin-film region, it is equal to $P_{\text{atm}} - P_{\text{cap}}$. This pressure difference drives the flow, and steady state happens when the pressure on both sides is equal (no heating case). In this experiment, the water droplet is deposited from a close distance (2 cm) on a dry, unheated microstructured surface to estimate the final wetted area and spreading time for a given droplet size and microstructure geometry.

To predict the spreading time of the deposited droplet on a microstructured surface, eq 1 is reformulated in a cylindrical coordinate and divided by porosity to estimate interstitial velocity, as shown below

$$\frac{dL}{dt} = \frac{KP_{\text{cap}}}{\varepsilon\mu L \ln \frac{L}{b}} \quad (19)$$

where L is the radius of the circular wetted region and b is the radius of the droplet region, as shown in eq 20 below

$$b = \left[\frac{3V_{\text{drop}}}{\pi} (2 - 3 \cos(\alpha) + \cos^3(\alpha)) \right]^{1/3} \sin(\alpha) \quad (20)$$

where α is the contact angle of the droplet region and is experimentally determined to be between 7° and 12° , as shown in panels b and c of Figure 18, respectively. Figure 17 illustrates the schematic of the droplet spreading problem.

The solution of eq 19 is shown in section S-5 of the Supporting Information. The permeability in this case is similar to the permeability presented in the previous section of this report. At the edge of the droplet, when $r = b$, the capillary pressure is equal to zero, and therefore, $h_{\text{eff}} = h$. On the other hand, at the edge of the wetted region at distance L , the capillary pressure is P_{avg} . The value of P_{avg} is used in eqs 12–14. After that, eq 17 is used to calculate h_{avg} to estimate permeability with the Byon and Kim model.³

The experimental procedure is similar to the experimental procedure presented in the Average Liquid Height section. The high-speed camera was set on 5000 frames per second. The needle height was kept at 2 cm to make the Weber number constant. For instance, the Weber number in our experiment was between 7.5 and 9 depending upon the droplet size. These values of the Weber number produce uncertainty in our experiments, which is taken into account in the droplet region contact angle (α). Figure 18 illustrates snapshots of the high-speed camera during liquid spreading to estimate the spreading time. It was observed that α is not constant and was changing from 7° (Figure 18b) to 12° (Figure 18c). This variation is due to initial droplet impingement (Weber number), which we tried to minimize in this experiment.

A total of 18 similar experiments were performed for six different samples to compare the spreading time to the model

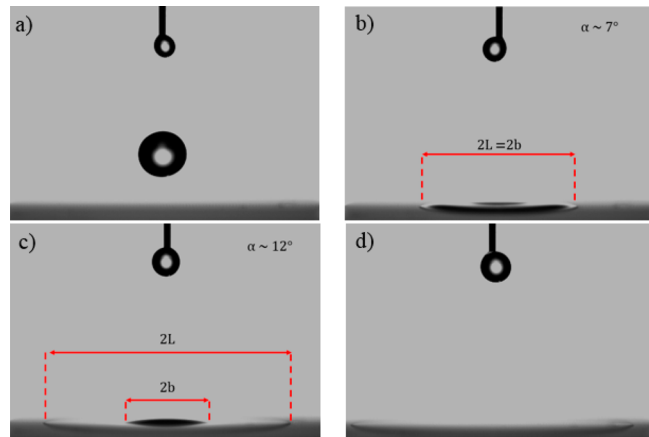


Figure 18. Snapshot of the high-speed camera for sample $d = 19$, $p = 51$, and $h = 35.6 \mu\text{m}$: (a) before impact, to measure the initial droplet volume, (b) $t = 0 \text{ ms}$, (c) $t = 30 \text{ ms}$, and (d) $t = 50.8 \text{ ms}$ (full spreading).

prediction using P_{avg} and $\alpha = 7^\circ$ and 12° , as shown in Figure 19 and Table 2.

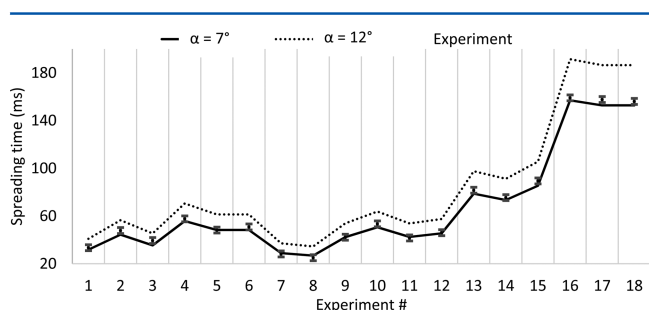


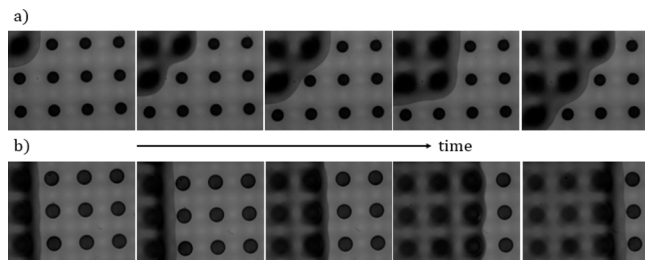
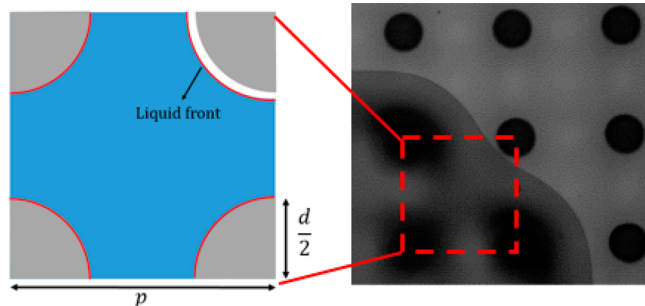
Figure 19. Comparison between the experimental spreading time and model prediction.

In comparison of the experimental results to the model prediction, the experimental results fit the model with $\alpha = 7^\circ$, which means that the model slightly underpredicts the spreading speed. The main reason is that the propagation mechanism in this case is different from that of the liquid rise experiment, as shown in Figure 20.

The proposed capillary pressure model in this paper was based on the propagation mechanism similar to Figure 20b, where the liquid front motion parallels the pillar direction, as in the case of liquid rise. In the case of droplet spreading, the liquid spread in all directions, which results in a microscale propagation mechanism similar to Figure 20a, and this leads to three wetted pillars, instead of two wetted pillars, per unit cell during microscale liquid propagation (Figure 21). As a result, P_{min} will be different, as shown below

Table 2. Experimental Results of the Spreading Time (ms) Using Different Size Droplets on Different Samples

experiment number	<i>d</i> (μm)	<i>p</i> (μm)	<i>h</i> (μm)	<i>V_i</i> (μL)	modeled spreading time ($\alpha = 12^\circ$) (ms)	modeled spreading time ($\alpha = 7^\circ$) (ms)	spreading time (experiment) (ms)
1	14	36	35.7	1.33	40.9	31.8	33.4
2				1.74	56.5	44.4	47.8
3				1.45	45.4	35.4	39.4
4	19	51	35.6	2.28	70.5	55.8	57.6
5				2.03	61.3	48.3	48.2
6				2.03	61.3	48.3	50.8
7	24	66	35.6	1.36	37.1	28.9	28.2
8				1.28	34.5	26.8	25
9				1.85	53.9	42.3	42.2
10	34	76	37.9	2.43	63.8	50.6	53.4
11				2.11	53.8	42.5	41.6
12				2.23	57.5	45.5	46
13	34	76	26.3	1.44	97.6	78.7	81.6
14				1.36	91.2	73.4	75.4
15				1.54	105.6	85.4	89.4
16	34	76	20.7	1.30	191.5	157	159
17				1.27	186.4	152.7	157.6
18				1.27	186.4	152.7	156

**Figure 20.** Propagation mechanism in (a) droplet spreading and (b) liquid rise.**Figure 21.** Schematic and microscope image of a unit cell that generates the minimum capillary pressure with three wetted pillars.

$$P_{\min 3} = \frac{\sigma \frac{3}{4} \pi d \cos \theta_{\text{pillar}} - d \sin \theta_{\text{adv}}}{p^2 - \frac{\pi d^2}{16}} \quad (21)$$

In comparison of the minimum capillary pressure when the liquid wets two pillars (P_{\min}) and three pillars ($P_{\min 3}$), $P_{\min 3}$ is 15–25% larger than P_{\min} for the pillar geometry used in our experiments. The average capillary pressure in the case of three wetted pillars is difficult to estimate because the microscale liquid front motion (x versus t) is unknown.

3. CONCLUSION

Liquid propagation in micropillar arrays has been studied in this paper, in which three main parameters (capillary pressure,

average liquid height, and contact angle on the pillar sidewall) were estimated and validated with experimental data. It was shown that the capillary pressure is not constant during liquid propagation, and therefore, an average capillary pressure model was provided on the basis of the maximum and minimum capillary pressures. The average liquid height in a unit cell, which is essential for permeability estimation, was modeled using the horizontal force balance analysis. A simple yet accurate model is developed. The contact angle on the pillar sidewall was debated for a long time in the literature, and we provided a physical model to predict that. The contact angle model was validated with literature interferometry results. The modeling results agree with liquid rise experiments with less than 10% error. Previous studies suggested a constant value of liquid sweeping scaling (β), and our results show that it is significantly affected by $h/(p-d)$. Also, droplet spreading on silicon micropillar arrays was modeled, where the spreading time and diameter were estimated and validated. It was shown that, as a result of different microscale propagation mechanisms, the capillary pressure in the droplet spreading case is higher than that in liquid rise, which stresses the importance of microscale propagation on macroscale propagation. This work provides a fundamental understanding of liquid propagation in micropillar arrays, which is important to design capillary-pumped devices.

ASSOCIATED CONTENT

S Supporting Information

The Supporting Information is available free of charge on the ACS Publications website at DOI: [10.1021/acs.langmuir.7b01090](https://doi.org/10.1021/acs.langmuir.7b01090).

Figures and equations for vertical force balance on the edge unit cell, steady-state contact angle on the pillar side, average capillary pressure, average liquid height in a unit cell of micropillar arrays, and droplet spreading (PDF)

AUTHOR INFORMATION

Corresponding Author

*E-mail: tjzhang@masdar.ac.ae.

ORCID®

Mohamed H. Alhosani: 0000-0001-5242-1120

Notes

The authors declare no competing financial interest.

ACKNOWLEDGMENTS

This work was supported by the cooperative agreement between the Masdar Institute of Science and Technology, United Arab Emirates, and the Massachusetts Institute of Technology (MIT), Cambridge, MA, U.S.A. (Reference 02/MI/MIT/CP/11/07633/GEN/G/00). It was also supported by the Abu Dhabi National Oil Company (ADNOC). The authors appreciate the early discussion with prof. Evelyn N. Wang at MIT and technical support from Leslie George at the Masdar Institute Clean Room.

REFERENCES

- (1) Wenzel, R. N. Resistance of Solid Surfaces to Wetting by Water. *Ind. Eng. Chem.* **1936**, *28*, 988–994.
- (2) Sangani, A. S.; Acrivos, A. Slow Flow Past Periodic Arrays of Cylinders with Application to Heat Transfer. *Int. J. Multiphase Flow* **1982**, *8* (3), 193–206.
- (3) Byon, C.; Kim, S. J. The Effect of Meniscus on the Permeability of Micro-Post Arrays. *J. Micromech. Microeng.* **2011**, *21*, 115011.
- (4) Horner, D.; Ravi, S.; Moghaddam, S. Monoporous Micropillar Wick Structures, II-Optimization & Theoretical Limits. *Appl. Therm. Eng.* **2014**, *73* (1), 1378–1386.
- (5) Raj, R.; Adera, S.; Enright, R.; Wang, E. N. High-Resolution Liquid Patterns via Three-Dimensional Droplet Shape Control. *Nat. Commun.* **2014**, *5*, 4975.
- (6) Ranjan, R.; Patel, A.; Garimella, S. V.; Murthy, J. Y. Wicking and Thermal Characteristics of Micropillared Structures for Use in Passive Heat Spreaders. *Int. J. Heat Mass Transfer* **2012**, *55* (4), 586–596.
- (7) Adera, S.; Antao, D.; Raj, R.; Wang, E. N. Design of Micropillar Wicks for Thin-Film Evaporation. *Int. J. Heat Mass Transfer* **2016**, *101*, 280–294.
- (8) Lu, H.; Yan, K.; Yan, J.; Wang, J.; Huang, B. Fabrication of Copper Micro-Tubes by Electroless Deposition with an Etched Porous Aluminum Template without Using Sensitization and Activation. *Mater. Chem. Phys.* **2008**, *110* (1), 136–139.
- (9) Piao, Y.; Lim, H.; Chang, J. Y.; Lee, W.-Y.; Kim, H. Nanostructured Materials Prepared by Use of Ordered Porous Alumina Membranes. *Electrochim. Acta* **2005**, *50*, 2997–3013.
- (10) Rahman, Md. M.; Ölçeroğlu, E.; McCarthy, M. Role of Wickability on the Critical Heat Flux of Structured Superhydrophobic Surfaces. *Langmuir* **2014**, *30* (37), 11225–11234.
- (11) Washburn, E. W. The Dynamics of Capillary Flow. *Phys. Rev.* **1921**, *17* (3), 273–283.
- (12) Xiao, R.; Enright, R.; Wang, E. N. Prediction and Optimization of Liquid Propagation in Micropillar Arrays. *Langmuir* **2010**, *26* (19), 15070–15075.
- (13) Xiao, R.; Wang, E. N. Microscale Liquid Dynamics and the Effect on Macroscale Propagation in Pillar Arrays. *Langmuir* **2011**, *27* (17), 10360–10364.
- (14) Tanner, H. L. The Spreading of Silicon Oil Drops on Horizontal Surfaces. *J. Phys. D: Appl. Phys.* **1979**, *12* (9), 1473.
- (15) Hale, R. S.; Bonnecaze, R. T.; Hidrovo, C. H. Optimization of Capillary Flow through Square Micropillar Arrays. *Int. J. Multiphase Flow* **2014**, *58*, 39–51.
- (16) Mai, T. T.; Lai, C. Q.; Zheng, H.; Balasubramanian, K.; Leong, K. C.; Lee, P. S.; Lee, C.; Choi, W. K. Dynamics of Wicking in Silicon Nanopillars Fabricated with Interference Lithography and Metal-Assisted Chemical Etching. *Langmuir* **2012**, *28* (31), 11465–11471.
- (17) Antao, D. S.; Adera, S.; Zhu, Y.; Farias, E.; Raj, R.; Wang, E. N. Dynamic Evolution of the Evaporating Liquid-Vapor Interface in Micropillar Arrays. *Langmuir* **2016**, *32* (2), 519–526.
- (18) Zhu, Y.; Antao, D. S.; Lu, Z.; Somasundaram, S.; Zhang, T.; Wang, E. N. Prediction and Characterization of Dry-out Heat Flux in Micropillar Wick Structures. *Langmuir* **2016**, *32* (7), 1920–1927.
- (19) Ravi, S.; Horner, D.; Moghaddam, S. A Novel Method for Characterization of Liquid Transport through Micro-Wicking Arrays. *Microfluid. Nanofluid.* **2014**, *17* (2), 349–357.
- (20) Ravi, S.; Horner, D.; Moghaddam, S. Monoporous Micropillar Wick Structures, I-Mass Transport Characteristics. *Appl. Therm. Eng.* **2014**, *73* (1), 1371–1377.
- (21) Ayon, A. A.; Chen, K.-S.; Lohner, K. A.; Spearing, S. M.; Sawin, H. H.; Schmidt, M. A. Deep Reactive Ion Etching of Silicon. *MRS Online Proc. Libr.* **1998**, *546*, 51–61.
- (22) Srivastava, N.; Din, C.; Judson, A.; Macdonald, N. C.; Meinhart, C. D. A Unified Scaling Model for Flow through a Lattice of Microfabricated Posts. *Lab Chip* **2010**, *10*, 1148–1152.